Arch Appl Mech
https://doi.org/10.1007/s00419-018-1362-1

ORIGINAL

A. Leontari · M. Apostolou

Linearised response of arched structures under pulse-type excitation

Received: 7 July 2017 / Accepted: 6 March 2018

Abstract Seismic response of masonry arches is examined in this study through analytical and numerical methods. Emphasis is placed on the low-amplitude levels where linearisation techniques may be efficient. When dealing with monumental arches of fragmented masonry, rocking rotation even in low levels is most often undesirable as it may lead to severe permanent displacements and dislocation of the arch axis, and sometimes to general instability of the structure. It is therefore of great importance to develop simplified procedures for estimating the levels of such low-amplitude arch response in earthquake-prone regions. Near-source ground excitation at the base of the structure is idealised with rectangular and cycloidal pulses. The analysis is limited to the prior-to-impact regime in which rocking occurs between successive fragments (voussoirs). This limitation does not prevent from extracting conclusions, as the prior-to-impact state is the most crucial to rocking response and it can determine whether the structure will undergo rocking vibration or eventually overturns. For simplicity, a specific kinematic mechanism of the fragmented arch, well known in the literature, is implemented throughout the study, thus allowing for comparison of the results with existing solutions. This idealisation is justified as the predominant mechanism from both previous analytical and experimental studies. A good correlation of the results between simplified closed-form solutions and rigorous semi-analytical methods is accomplished. Moreover, these results are also quite close to those of the 2D finite element analysis.

Keywords Masonry arches · Idealised pulses · Rocking · FE analysis

1 Introduction

Arched masonry structures (such as vaulted bridges and cathedral domes) are an important part of the cultural heritage worldwide. Although nowadays construction of this kind of structures is quite rare, the necessity of their preservation has spurred many researchers to thoroughly investigate collapse mechanisms, as well as ways to protect them against natural hazards and decay through time. In this context, Coulomb's [1] and then Couplet's [2] studies are highlighted, confirming what master builders knew by empirical intuition: arch equilibrium is a pure geometric problem rather than a problem of strength of material.

Early studies on the stability of masonry arches under gravity loads were made by Heyman [3–5]. The equilibrium approach proposed in these studies stemmed from the plastic analysis principles of steel structures. Within the framework of the limit state analysis, Heyman established three fundamental assumptions concerning material properties of stone blocks: (a) infinite compression strength, (b) zero tensile strength and (c) coefficient of friction at the interface of subsequent voussoirs adequate large so that sliding be avoided. As a consequence, failure of the arch may occur through the formation of four hinges that turns the arch into a mechanism.

A. Leontari (✉) · M. Apostolou
School of Civil Engineering, National Technical University, Athens, Greece
E-mail: airinaleo@gmail.com

Published online: 15 March 2018

Motivated by Heyman's fundamental work, Clemente extended the static equilibrium approach to incorporate earthquake lateral loads. In this way, the arch is considered to be subjected to a combination of constant horizontal and vertical acceleration (earthquake and gravity load, respectively). Then equivalent static analysis is performed to derive minimum levels of ground acceleration required to collapse the arch. It is denoted, however, that this pseudo-static method actually provides the minimum peak ground acceleration required to initiate rocking motion and transform the arch into a mechanism. It depends upon the dynamic properties of the structure and the excitation characteristics whether the structure safely experiences rocking or eventually collapses.

Oppenheim was the first one to incorporate the time-dependent nature of dynamic loading (e.g. earthquake) into the analysis of the masonry arch. In his pioneering study [6], Oppenheim was inspired by Housner's work on freestanding rigid blocks rocking on an accelerating base [7] and treated the arch as a rigid body assembly subjected to ground motion, through idealised pulses. This typical, circular arch consists of seven voussoirs, each one obeying Heyman's postulates. When subjected to dynamic loading, the rigid blocks may rock one to the other about fixed points, and the arched structure becomes a four-hinge mechanism with one degree of freedom. Among all the kinematically admissible mechanisms (each one is characterised by a different equation of motion, and corresponding to a different level of minimum horizontal ground acceleration for the onset of the mechanism motion), Oppenheim addresses the one which is associated with the lowest such minimum $\ddot{x}_g$ for the onset of motion, namely the governing mechanism. Evidently, the dynamic response under base excitation is a geometrical problem (characterised by the thickness ratio t/R and the angle of embrace β) and depends on initial conditions.

Clemente [8] implemented time-domain numerical analysis to compute the dynamic response of the masonry arch once the pseudo-statically predicted ground acceleration required for rocking initiation is exceeded. He examined arch response during free vibration as well as under rectangular and sinusoidal pulses. Emphasis was placed given on kinematic characteristics (frequency and amplitude) without yet taking impact and damping into consideration. De Lorenzis et al. [9] moved a step further by calculating analytically the arch response after the first impact of rigid blocks, when hinges reopen and a new four-link mechanism is formed.

As already discussed, Oppenheim did not consider a continuous monolithic arch with zero tensile strength but rather a circular arch that consists of seven voussoirs. He further simplified the rocking arch to a four-hinge mechanism, whereas the location of the hinges is dictated by the governing mechanism (i.e. the one corresponding to the minimum peak ground acceleration). This theoretical prediction of the rigid body mechanism once rocking occurs was confirmed experimentally by DeJong et al. [10]. Recently, Alexakis and Makris [11] revisited the analysis of a continuous monolithic circular arch through limit equilibrium approach. The locations of the hinges is in close agreement to those predicted by Oppenheim.

2 Statement of the problem

Consider the model illustrated in Fig. 1. Originally, the arched structure complies with the supporting base in a purely horizontal motion. When a crucial acceleration is reached, it launches a four-link rocking mechanism. Impacts may occur at four pivot points (A, B', C', D) where hinges are formed. It is assumed thereafter, that hinge formation cannot take place in any other point along the arch. In view of this postulation the system can be simplified as a single degree of freedom. In accordance with the Oppenheim's model [6], the geometric characteristics are: (a) the angle of embrace $\beta = 157.5°$, (b) the centreline radius $R = 10\,\text{m}$ and (c) the ratio $t/R = 0.15$. Following Heyman's assumptions [3], the stone material of the arched structure is of infinite compressive strength, zero tensile strength and a large coefficient of friction to avoid entering the sliding mode at any instant in the rocking motion. In addition, it is assumed that hinges locations are predefined.

2.1 Kinematics of arch response

During dynamic motion, a hinge point may move along the arch axis; therefore, different instantaneous kinematic mechanisms are being developed. The governing kinematic mechanism according to Oppenheim [6] is presented in Fig. 1. This is the one that yields the lowest possible horizontal ground acceleration needed to set the arch to motion, and was chosen as the case study in the present work. A simplified form of the arch in its initial and displaced state is presented in Fig. 2, depicting only the links of the three parts (AB, BC and CD) formed before and after hinges (A, B, C, D) are open. Links AB and CD perform rotational motion

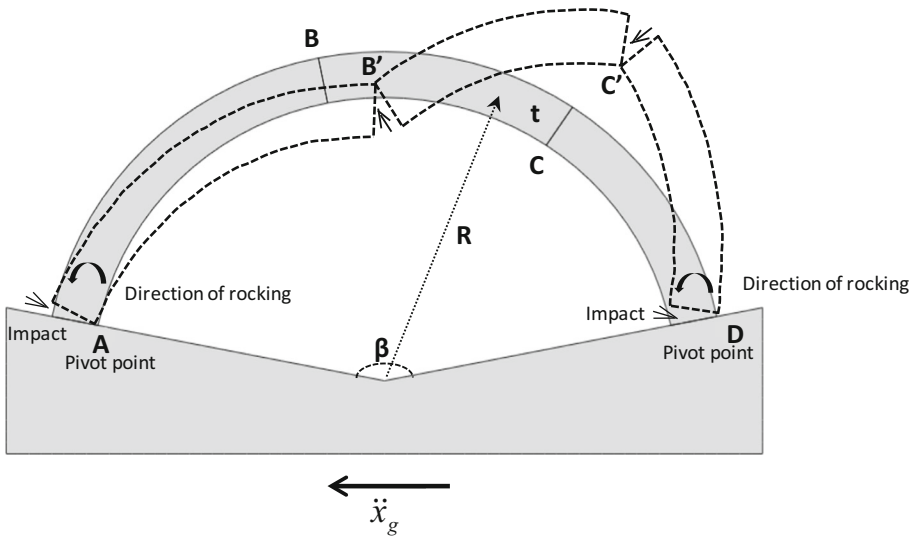

Fig. 1 Rocking arch on a rigid oscillating base: configuration of the system

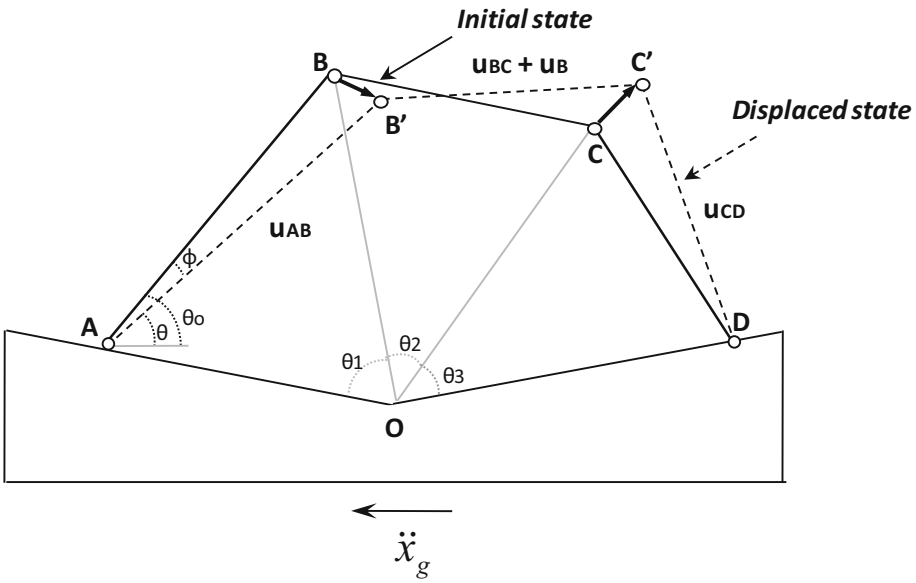

Fig. 2 Kinematics of mechanism motion as linkage synthesis

(u_{AB}, u_{CD}) considering A and D fixed. On the other hand, link BC performs a combination of rotational (u_{BC}) and translational (u_B) motion. Considering combined motion, the total kinetic energy of the rigid body at each moment is the sum of (a) the translational component and (b) the rotational component about the instantaneous pole. The rotation of each link θ_i measured anticlockwise from the horizontal, as well as rotation $\varphi = (\theta_0 - \theta > 0)$ with respect to the original geometry fully determine the motion. The presented kinematic mechanism is the result of the base acceleration to the left $(\ddot{x}_g < 0)$, causing a positive rotation (φ) of the arch which initially will rock to the right.

2.2 Methods of analysis

The response of such a complicated dynamic nonlinear system may be investigated with various analysis procedures which can be grouped into two categories: (a) analytical or semi-analytical methods and (b) numerical methods with finite elements. In this study, both categories are employed. With regard to the analytical

treatment, the Lagrangian method is adopted to derive the equation of motion that describes this kinematic system [6,9]. To further reduce the complexity of the problem, linearisation of the nonlinear equation of motion is necessary. Whenever a closed-form solution of equation of motion is not feasible, a general software system for mathematical applications "Mathematica" is utilised to compute the response.

On the other hand, numerical analysis is accomplished by using the sophisticated code *Abaqus* and by applying the explicit integration algorithm for solving the nonlinear dynamic response of the system in the time domain. Two-dimensional finite element (FE) analysis is performed assuming that hinges open at specific and fixed points (A, B, C, D). For the FE model, plane strain elements are used. Each block is idealised as rigid, by using a large enough modulus of elasticity ($E = 10\,\text{GPa}$), characterised by density $\rho = 2.2\,\text{t/m}^3$. The base is also considered to be rigid by adopting concrete elastic values (elastic modulus, $E = 30\,\text{GPa}$ and density, $\rho = 2.5\,\text{t/m}^3$). A sophisticated contact algorithm is utilised for modelling contact interface at hinges sections, thus allowing for separation but not for sliding. Hence, the coefficient of friction is adequately large ($\mu = 0.7$). Different types of pulses are imposed to the bottom surface of the base to represent seismic excitation. The major task of the finite element analysis is to evaluate the efficiency of the linearisation techniques in predicting the nonlinear response.

2.3 Equation of motion

As already discussed, the Lagrangian method is a convenient tool for the analysis of the above dynamic system. In its general form:

$$\frac{\mathrm{d}}{\mathrm{d}t}\left(\frac{\partial T}{\partial \dot{\theta}} - \frac{\partial T}{\partial \theta} + \frac{\partial V}{\partial \theta} = Q\right) \tag{1}$$

in which T is the kinetic energy of the system, V the potential energy and Q the generalised forces. For this single-degree-of-freedom system, the angle $\theta = \theta_{AB} = \theta_0$ is chosen arbitrarily and without violating the constraint, as the Lagrangian independent variable (coordinate). The complete expression of these values as a function of θ is given by Oppenheim [6]. For compactness, these formulations are not retyped herein. Finally, substitution of T, V and Q to Eq. (1) leads to the general nonlinear equation of motion as follows:

$$M(\theta)\ddot{\theta} + L(\theta)\dot{\theta}^2 + F(\theta)g = p(\theta)\ddot{x}_g \tag{2}$$

where the coefficients $M(\theta)$, $L(\theta)$, $F(\theta)$, $P(\theta)$ are nonlinear equations of θ given below after replacing $f_{xy} = m_{xy}\bar{r}_{xy}^2 + I_{xy}$:

$$M(\theta) = f_{AB} + f_{BC}\theta r_{BC}^2 + f_{CD}\theta'^2_{CD} + m_{BC}\left[AB^2 + 2AB\bar{r}_{BC}\theta'_{BC}\cos(\theta - \theta_{BC} - \psi_{BC})\right] \tag{3a}$$

$$L(\theta) = f_{BC}\theta'_{BC}\theta''_{BC} + f_{CD}\theta'_{CD}\theta''_{CD} + m_{BC}AB\bar{r}_{BC}\left[\theta''_{BC}\cos(\theta - \theta_{BC} - \psi_{BC}) - \theta'_{BC}(1 - \theta'_{BC})\sin(\theta - \theta_{BC} - \psi_{BC})\right] \tag{3b}$$

$$F(\theta) = m_{AB}\bar{r}_{AB}\cos(\theta + \psi_{AB}) + m_{BC}\left[AB\cos\theta + \bar{r}_{BC}\theta'_{BC}\cos(\theta_{BC} + \psi_{BC})\right] + m_{CD}\bar{r}_{CD}\theta'_{CD}\cos(\theta_{CD} + \psi_{CD}) \tag{3c}$$

$$P(\theta) = m_{AB}\bar{r}_{AB}\sin(\theta + \psi_{AB}) + m_{BC}\left[AB\sin\theta + \bar{r}_{BC}\theta'_{BC}\sin(\theta_{BC} + \psi_{BC})\right] + m_{CD}\bar{r}_{CD}\theta'_{CD}\sin(\theta_{CD} + \psi_{CD}) \tag{3d}$$

Their physical interpretation has been approached by Oppenheim [6]. Equation 2 is valid only when the angle $\theta < \theta_0$, meaning that the computation of the rocking angle θ is limited to the prior-to-impact state. Once θ_0 is exceeded, a new kinematic mechanism is generated which requires a fundamentally different analytical treatment.

3 Linearisation techniques of arch response

The coefficients $M(\theta)$, $L(\theta)$, $F(\theta)$, $P(\theta)$ in Eq. (2) may be divided by $M(\theta)$ reformulating the equation of motion as follows:

$$\ddot{\theta} + b(\theta)\dot{\theta}^2 = c(\theta)g + d(\theta)\ddot{x}_g \tag{4}$$

in which $b(\theta) = L(\theta)/M(\theta)$, $c(\theta) = F(\theta)/M(\theta)$ and $d(\theta) = P(\theta)/M(\theta)$.

This is the general form of the equation of motion, which is nonlinear as coefficients of Eq. (4) are complicated functions of the angle θ. For small variations, however, it can be postulated that these coefficients remain constant [6]. Searching out for the solution of Eq. (4), the following transformation is introduced.

$$\theta(t) = \frac{1}{b}\log(u(t)) \tag{5}$$

The left side of Eq. (4) may be expressed in terms of a new variable u as:

$$\ddot{\theta} + b\dot{\theta}^2 = \frac{1}{b}\frac{\ddot{u}}{u} \tag{6}$$

Then, the equation of motion yields:

$$\frac{1}{b}\frac{\ddot{u}}{u} = cg + d\ddot{x}_g \tag{7}$$

Equation (7) may now be written in a standard form of a linear differential equation of 2nd degree:

$$\ddot{u}(t) - b(|c|g + d\,\ddot{x}_g)u(t) = 0 \tag{8}$$

3.1 Equation of motion in terms of rotation φ

Alternatively, the equation of motion can explicitly be expressed in terms of φ (defining $\varphi = \theta_0 - \theta$):

$$M(\varphi)\ddot{\varphi} + L(\varphi)\dot{\varphi}^2 + F(\varphi)g = P(\varphi)\ddot{x}_g \tag{9}$$

Coefficients F, P are Taylor series expansions about φ and are approximated by keeping only the first-order terms. Clearly, an approximate rather than a detailed solution is sought. In a similar algebraic procedure to that when the variable θ is regarded, Eq. (9) finally yields:

$$2\ddot{\varphi} - b\dot{\varphi}^2 - c\varphi - h = 0 \tag{10}$$

The above is applicable only for small values of rotation ϕ; otherwise, the expansion does not converge. The general solution of Eq. (10) is unveiled below and it can be characterised as a differential equation in terms of the phase space variables $(\dot{\varphi}, \varphi)$.

$$\dot{\varphi}^2 = \frac{c + bh}{b^2}(e^{b\varphi} - 1) - \frac{c\varphi}{b} \tag{11}$$

3.2 Onset of mechanism motion

Recall now Eq. (2). The ground acceleration amplitude required to transform the arch into a four-link mechanism is extracted from this equation by applying the criterion for incipient rocking: $\ddot{\theta} = \dot{\theta} = 0$ [12,13]. Hence, for a ground acceleration larger than $|\ddot{x}_g| = F(\theta)/P(\theta)$, the developing inertia forces set the arch on rocking. From that point on, equilibrium becomes unstable and overturning is possible. Nevertheless, there is a thin zone, in terms of the angle θ, in which the structure can safely undergo rocking. This zone is bounded by critical values of $\theta_{\max} = \theta_0$ and $\theta_{\min}$. The latter is associated with a critical point that Oppenheim called it the "non-recovery" point, as it determines whether the structure will return to its initial position (recovery region) or will eventually collapse (non-recovery region). Energy approach can provide levels of this lower value of θ. Similarly, if the independent variable φ is chosen, the rocking criterion becomes $\ddot{\varphi} = \dot{\varphi} = 0$, and through Eq. (9), the critical ground acceleration becomes $|\ddot{x}_g| = F(\varphi)/P(\varphi)$. Then, the critical rotation separates safe from overturning response. All the above are portrayed in Fig. 3, using the numerical example of the preceding. Hence, for a rocking rotation larger than $\varphi = 0.07$ rad, the gravitational force is converted from restoring to overturning, meaning that it destabilises structural equilibrium. This conclusion results from the fact that the coefficient $F(\varphi)$ normalised to its value, becomes negative after the non-recovery point as shown in Fig. 3. On the contrary, the coefficient $P(\varphi)$ normalised to its value reveals that the ground acceleration destabilises the four-link mechanism from the beginning, having its contribution increasing almost linearly in relation to the rotation φ.

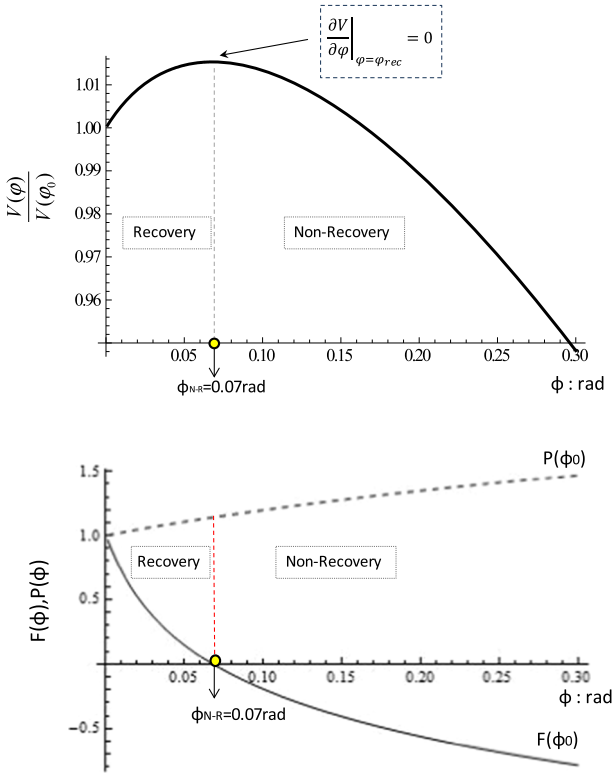

Fig. 3 Potential energy normalised to its maximum value along with the representative coefficient F and coefficient P defined by the non-recovery point

4 Linearised response under pulse-type motion: numerical examples

4.1 Constant acceleration pulse

At first, the arch is subjected to a constant acceleration pulse $\ddot{x}_g = -\lambda g$. A negative (positive) sign of the ground acceleration denotes clockwise (anticlockwise) rocking rotation (φ) of the structure. Recalling equation of motion in terms of u [Eq. (8)] and substituting $\ddot{x}_g = -\lambda g$ and $\tilde{c} = (\lambda d - c)g$, it yields:

$$\ddot{u}(t) + b\,\tilde{c}\,u(t) = 0 \tag{12}$$

which is a second-order differential equation with fixed coefficients and its solution can be built up by a linear combination of trigonometric functions.

$$u(t) = A_1 \cos\left(\sqrt{b\tilde{c}}\,t\right) + A_2 \sin\left(\sqrt{b\tilde{c}}\,t\right) \tag{13}$$

where A_1, A_2 are constants. It is evident that:

$$u(t) = c_2 \cos\left(\sqrt{b\tilde{c}}(t - c_1)\right) \tag{14}$$

where c_1, c_2 are new constants that can be defined from initial conditions.

Equation (14) in combination with the transformation of Eq. (5) yields the solution in terms of the angle $\theta(t)$.

$$\theta(t) = c_2 + \frac{\log\left(\cos\left(\sqrt{b\tilde{c}}(t - c_1)\right)\right.}{b} \tag{15}$$

At $t = 0$ angle θ_{AB} is:

$$\theta(0) = c_2 + \frac{\log\left(\cos\left(\sqrt{b\tilde{c}}(-c_1)\right)\right.}{b} \tag{16}$$

Or

$$\theta_0 = c_2 + \frac{\log(\cos c_1\sqrt{b\tilde{c}})}{b} \tag{17}$$

Derivation of Eq. (15) provides the rotational velocity:

$$\dot{\theta}(t) = -\sqrt{\frac{c}{b}}\tan\left(\sqrt{b\tilde{c}}(t - c_1)\right) \tag{18}$$

At $t = t_0$, the rotational velocity is zero; therefore,

$$\dot{\theta}(0) = 0 = \tan\left(\sqrt{b\tilde{c}}(-c1)\right) => c_1 = 0 \tag{19}$$

Substitution of the value of c_1 to Eq. (17) allows for c_2 to be calculated:

$$\theta(0) = c_2 + \frac{\log\left(\cos\left(\sqrt{b\tilde{c}}\,0\right)\right.}{b} = \theta_0 => c_2 = \theta_0 \tag{20}$$

Eventually the analytical solution yields in terms of θ:

$$\theta(t) = \theta_0 + \frac{\log\left(\cos\left(\sqrt{b\tilde{c}}t\right)\right)}{b} \tag{21}$$

Numerical implementation is presented next based on the above solution. The coefficients M, L, F, P of the equation of motion are calculated considering the aforepresented numerical example (geometric characteristics: arch radius $a = 10\,\text{m}$, angle of embrace $\beta = 157.5°$, ratio thickness/radius $(t/R) = 0.15$). For this specific case, Eqs. (2) and (4) become, respectively:

$$4370\,\ddot{\theta} + 59249\dot{\theta}^2 - 87.7g = 239\,\ddot{x}_g \tag{22}$$

$$\ddot{\theta} + 13.56\dot{\theta}^2 - 0.02g = 0.055\,\ddot{x}_g \tag{23}$$

It is noted the computed response is associated with the specific kinematic mechanism adopted so far. (A different kinematic mechanism would respond to different values of these coefficients.)

Figure 4 depicts the development of rotation θ_{AB} over time for different constant pulses based on the above equation. Initially, the static angle of the link AB is $\theta_0 = 0.8972\,\text{rad}$ and consequently the starting point of all curves. The ground acceleration amplitude that transforms the arch into a four-link mechanism is extracted from Eq. (22) by applying the criterion for incipient rocking: $\ddot{\theta} = \dot{\theta} = 0$. For a ground motion larger than $|\ddot{x}_g| = F(\theta)/P(\theta) > 0.37g$, the developing inertia forces set the arch on rocking. From that point on, equilibrium becomes unstable and overturning is inevitable as depicted from the time histories of Fig. 4.

This value of φ corresponds to $\theta = \theta_{\min} = 0.8272\,\text{rad}$ (in displaced state) and it is highlighted in Fig. 4 with black dashed line. Curves that cross that line (i.e. $|\ddot{x}_g| = 0.39g, 0.45g, 0.56g, 0.61g, 0.71g$) represent arches that fail as rotation θ drops below the critical value. In contrast, curve $0.37g$ represents a rocking arch in marginal equilibrium. The stronger the impulse the sooner the arch collapses.

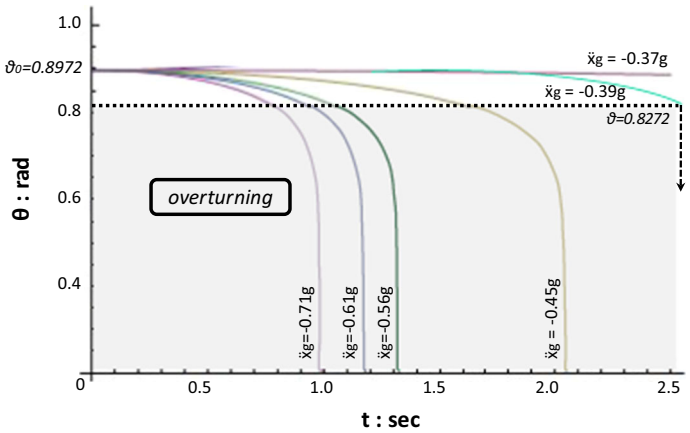

Fig. 4 Time history of angle θ_{AB} for different levels of ground excitation

4.2 One-sine pulses

Herein, the linearised equation of motion is readjusted for a sinusoidal ground motion. Cycloidal pulse of type A approximates a forward pulse of near fault ground motion and is chosen over one cosine pulse (type B Pulse) because of its more destructive effects [14]. Within the limits of the linear approximation and for a ground acceleration,

$$\ddot{x}_g = -a_\mathrm{p} \sin(\omega_\mathrm{p} t) \tag{24}$$

(where a_p and ω_p are the acceleration amplitude and the angular frequency of the pulse, respectively, t is the time and the minus sign designates positive rotation φ), the governing Eq. (8) becomes:

$$\ddot{u}(t) - b(|c|g - da_\mathrm{p} \sin(\omega t))u(t) = 0 \tag{25}$$

A suitable transformation of variable [Eq. (26)] is used to convert q. (25) to a linear second-order homogeneous differential equation, similar to that are well known from the literature Mathieu equation [Eq. (27)].

$$\omega t = 2x + \frac{\pi}{2} \tag{26}$$

$$\ddot{u}(x) + (A - 2Q\cos(2x))u(x) = 0 \tag{27}$$

Mathieu equation commonly occurs in nonlinear vibration problems, (a) in systems in which there is periodic forcing and (b) instability studies of periodic motions in nonlinear autonomous systems [15,16]. Recall the case of a pendulum whose support is periodically forced in a vertically direction as a typical example. Obviously, the coefficient of the differential equation is periodic without entailing that the equation possesses only periodic solutions. Only for specific values of the constants A, Q (which are often referred as characteristic number and parameter, respectively) a periodic solution is achieved. Both of them are expressed in terms of excitation parameters and of the coefficients of the equation of motion (b, c, d) [Eqs. (28–30)]. As already mentioned, the latter are complicated functions of angle θ, but assuming small variations of θ, they remain constant. Adopting initial formulae, they may be rewritten as in Eqs. (29–30). It is noted that A encompasses the potential energy which is proportional to θ at any displaced configuration of the arch. Similarly, Q describes the applied external force, emphasised on the excitation amplitude a_p.

$$A = \frac{4gbc}{\omega^2} \quad Q = \frac{2a_\mathrm{p}bd}{\omega^2} \tag{28}$$

$$A = \frac{4gL(\theta)F(\theta)}{[\omega M(\theta)]^2} \quad \text{Or} \quad A = 2EF(\theta)g \tag{29}$$

$$Q = \frac{2a_\mathrm{p}L(\theta)P(\theta)}{[\omega M(\theta)]^2} \quad \text{Or} \quad Q = EP(\theta)a \tag{30}$$

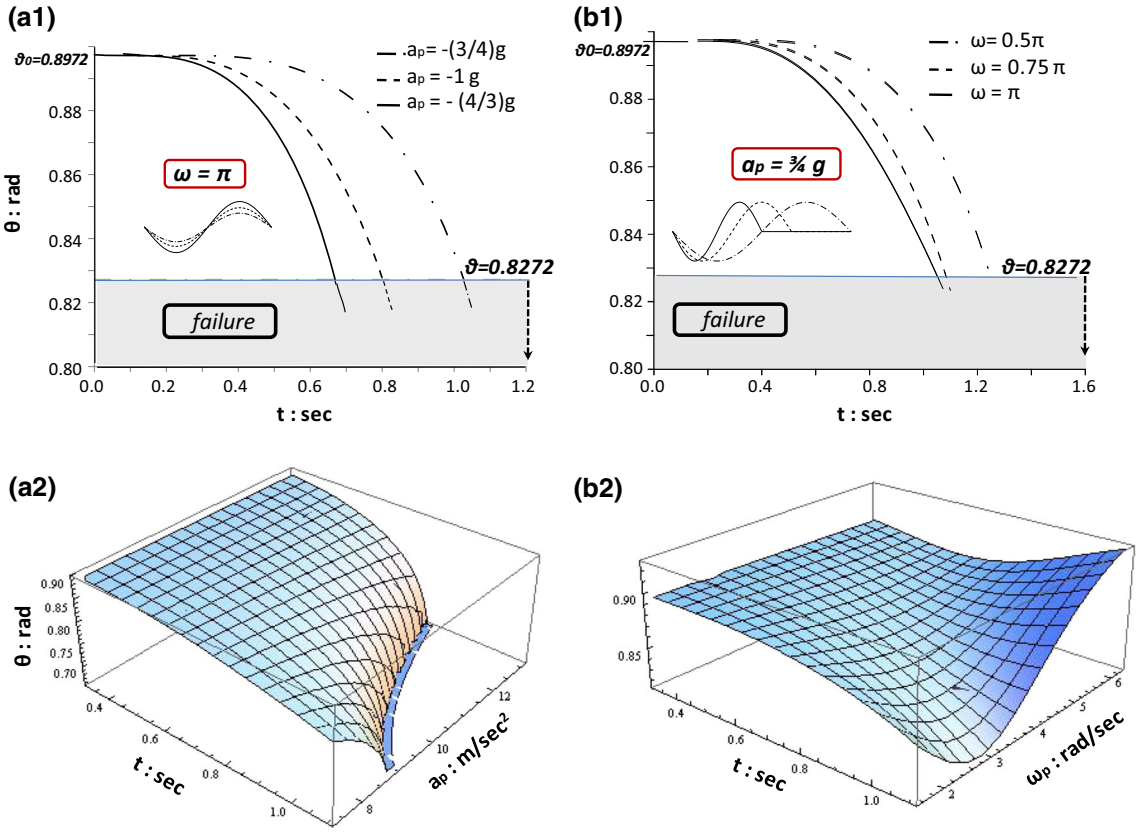

Fig. 5 Effect of the acceleration amplitude a_{p} ($\mathbf{a_1}$, $\mathbf{a_2}$) and of the excitation frequency ω_{p} ($\mathbf{b_1}$, $\mathbf{b_2}$) on the rocking response presented in 2D and 3D

where

$$E = \frac{2L(\theta)}{[\omega M(\theta)]^2}$$

According to superposition principle, Eq. (27) possesses a solution which is a linear combination of two independent solutions, $u_1(x)$ and $u_2(x)$. This solution is obtained below:

$$u(x) = c_1 u_1(x) + c_2 u_2(x) \tag{31}$$

The arbitrary constants c_1 and c_2 are defined by the boundary conditions supposing that for $x = x_0$, the general solution is $u(x) = u(x_0)$ and its derivative is $u'(x_0) = 0$.

To be more specific, the example of the aforediscussed arch will be used. The numerical solution of Eq. (31) is obtained with a computational algorithm. It is omitted, however, due to the intricacy of the coefficients $c_{1,2}$ and of the solutions $u_{1,2}$. It is worth mentioning that no periodic solutions correspond to this system. For convenience, however, the differential equation [Eq. (27)] can be presented numerically. Hence, for various sine pulses (a_{p}, ω_{p}) it yields:

$$\ddot{u}(x) + \frac{1}{\omega^2}(10.6 - 2.96 a_{\mathrm{p}} \cos(2x))u(x) = 0 \tag{32}$$

As already discussed, the motion initiates when the ground acceleration $\ddot{x}_g$ exceeds the value of 0.37g. For the sine pulse case, the aforementioned applies when $a_{\mathrm{p}} \sin(\omega_{\mathrm{p}} t) > |-0.37|g \Rightarrow t_0 = \frac{1}{\omega_{\mathrm{p}}} \sin^{-1}[\frac{(|-0.37|g)}{\alpha_{\mathrm{p}}}]$. At that time, hinges are formed, and as a result, the arch is transformed into a mechanism. The arch rocking response can be further described with the excitation parameters, the acceleration amplitude (a_{p}) and the excitation frequency ($\omega_{\mathrm{p}} = 2\pi / T_{\mathrm{p}}$). It is therefore interesting to develop diagrams of rotation θ_{AB} for different levels of the former parameters (Fig. 5). Thus, the way the pulse characteristics affect the overturning response

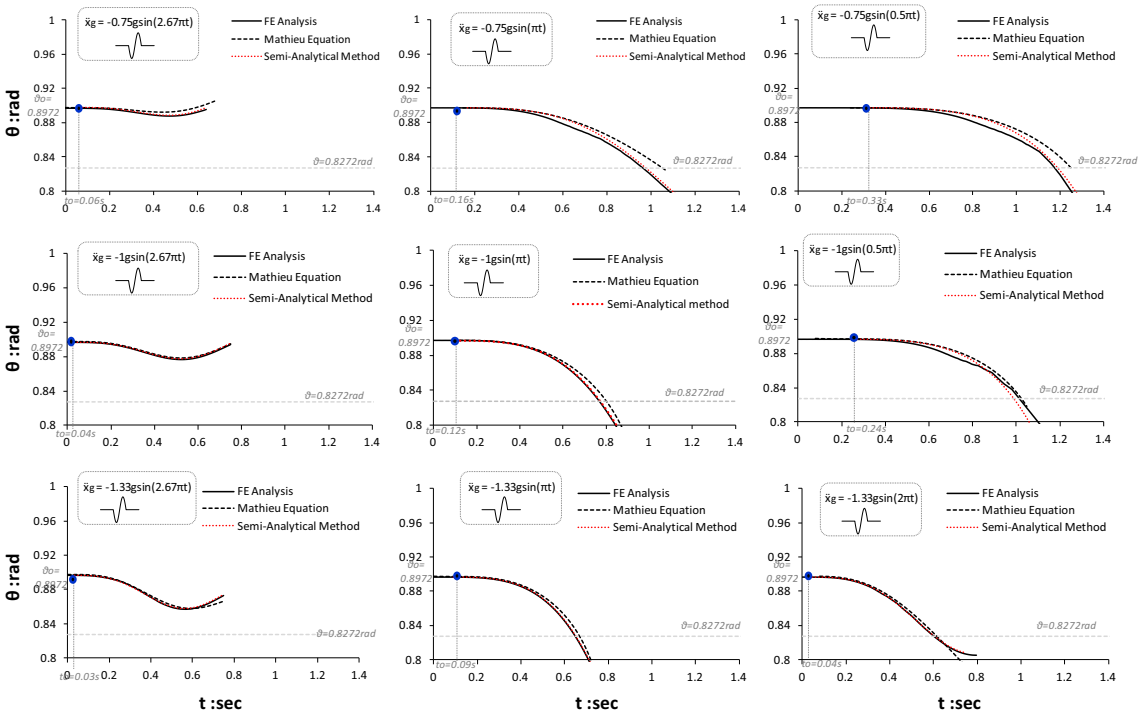

Fig. 6 Time histories of the angle θ_{AB} under one-sine pulse base excitation: (line 1) $a_p = -0.75g$, $T_p = 0.75, 2, 4$ s, (line 2) $a_p = -1g$, $T_p = 0.75, 2, 4$ s, (line 3) $a_p = -1.33g$, $T_p = 0.75, 1, 2$ s: comparison between finite element analysis and linearised analytical solutions (semi-analytical solution of Eq. (9) and closed-form solution with Mathieu equation)

is analysed separately. Notably, the selected pulses to be examined can adequately resemble recorded time histories of zero final ground velocity. In the first case, the excitation frequency remains constant and equal to $\omega_p = \pi$ ($T_p = 2$ s), whereas the acceleration amplitude fluctuates between $-(4/3)g$ to $-1g$ and $-0.75g$ (Fig. 6a$_1$). Evidently, the detrimental effect of the increasing a_p is clear as higher values lead more rapidly the arch to overturning (when the angle θ_{AB} exceeds the critical value of 0.8272 rad as mentioned above). For the most unfavourable case of the maximum $a_p = -(4/3)g$, the system is set into motion at $t_0 = 0.089$ s and overturning occurs at $t_{over} = 0.67$ s, at the second quarter of the pulse, whereas, for the other two levels of the acceleration amplitude, the motion onsets later at $t_0 = 0.12$ for $a_p = -1g$ and at $t_0 = 0.16$ s for $a_p = -0.75\,g$, and collapse time is defined at $t_{over} = 0.8$ (second quarter of the pulse), 1.05 s (third quarter of the pulse), respectively. In the second case, as shown in Fig. 6b, decreasing the ω_p from π ($T_p = 2$ s) to 0.75π ($T_p = 2.66$ s) and 0.5π ($T_p = 4$ s) (consequently increasing the excitation period T_p) and keeping constant the acceleration amplitude $a_p(= -3/4g)$ affects favourably the overturning response. Additionally, for all the examined cases, the results indicate that the arch rocks and collapses straightforward to the right, with no impacts to occur. 3D diagrams presented in Fig. 5b$_1$, b$_2$ are constructed to give insight of the predicted collapse mechanism.

Initially, the equation of motion is transformed for sinusoidal pulses into a Mathieu kind differential equation. Appropriate solution of this equation is found corresponding to this specific arch geometry [Eq. (32)]. In this respect, the computed time history of angle θ_{AB} for various one-sine pulse excitations with period ranging from $T_p = 0.75$ s to 4 s is presented in Fig. 6. The study of the impulse response is feasible till the first impact. Alternatively, the arch response under the same set of one-sine pulses may be repeated by implementing two additional methods: (a) a semi-analytical solution, in which the linearised equation of motion of Eq. 9 is solved iteratively through a numerical solver available in Mathematica code and (b) two-dimensional finite element analysis using Abaqus code. The results are comparatively portrayed in Fig. 6 along with those extracted from Mathieu equation. The comparison among the three methods proves to be remarkably good indicating the validity of the linearisation techniques. Nevertheless, as the finite element method provides rigorous solution for the four-link mechanism it still remains to be checked the accuracy of this simplified model.

In the preceding, Mathieu equation has been proved a useful tool to extract closed-form solutions for low amplitudes of rocking. It is also reminded that in this series of analyses, a unique value of the ratio t/R was

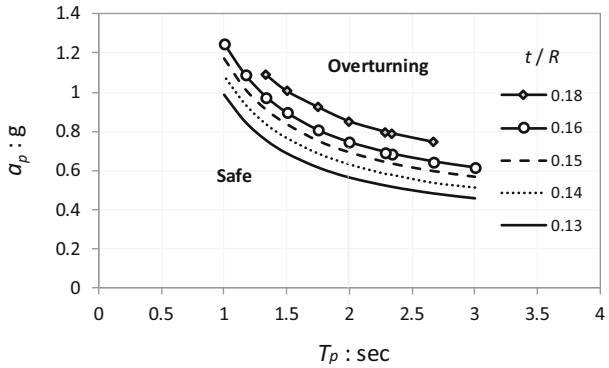

Fig. 7 Safe and overturning region formed by acceleration period pairs under sine pulses for different arches. Safe mode refers to the first impact moment. Overturning after one impact cannot be excluded

considered ($t/R = 0.15$). Simplified analysis of the rocking response based on Mathieu equation is extended next, by introducing more values of the ratio t/R. As before, the arched structure is subjected to cycloidal pulse-type excitation at the base. Whether the structure can safely experience rocking vibration or immediately collapses is illustrated with the overturning spectra of Fig. 7. For lower values of the period T_p, higher values of the acceleration amplitude are required to overturn the arch. In addition, for a specific period T_p, the higher the ratio t/R is, the higher the minimum acceleration is required to collapse. A long-period pulse ($T_\mathrm{p} = 2\,\mathrm{s}$ or $\omega_\mathrm{p} = \pi$ rad) is chosen from Fig. 7 as suitable to enlighten the rocking response at marginal equilibrium (Fig. 8). Time histories of the normalised angle θ_{AB}, the normalised rotation φ and the phase portrait confirm the influence of the geometrical parameters on the arch limit response. The heavier arch ($t/R = 0.18$) sustains larger rotations which is a rational conclusion given the larger inertia.

4.3 Rectangular pulses

The two-step rectangular pulse as an excitation to study the arch rocking response was introduced by Oppenheim [6]. Later, this extreme pulse was also used by De Lorenzis et al. [9]. In this context, the time history of the acceleration consists of a large negative pulse ($a_\mathrm{p} = -1g$) of duration t_p, followed by a smaller positive pulse of half magnitude ($a_\mathrm{p} = 0.5g$) and of double duration $2t_\mathrm{p}$. These pulse shape parameters lead to zero terminal ground velocity (Fig. 9). Two different values of the duration t_p have been adopted by Oppenheim, namely 0.40 and 0.44 s. These values of t_p are also applied herein so that comparative results can be extracted. General remarks for both cases regard mainly the movement of the base. The maximum value of the base velocity occurs when the acceleration changes sign, and it vanishes at the end of the pulse. On the other hand, the displacement time history indicates the change in curvature with the sign change and a residual displacement after the end of the pulse.

A computational solution of the equation of motion in terms of rotation φ (Eq. 9) is accomplished with *Mathematica* code, after properly adjusting the coefficient $P(\varphi)$ to implement ground shaking idealised with the two rectangular pulses illustrated in Fig. 9.

$$445\ddot{\varphi} - 6017.75\dot{\varphi}^2 + 87.86 = (-1g)(-237.45) \quad 0 \le t \le t_\mathrm{p} \tag{33}$$

$$445\ddot{\varphi} - 6017.75\dot{\varphi}^2 + 87.86 = (+0.5g)(-237.45) \quad t_\mathrm{p} \le t \le 3t_\mathrm{p} \tag{34}$$

The results obtained with the above method along with the results derived by Oppenheim are portrayed in Fig. 10. Moreover, the finite element method through *Abaqus* code is implemented to evaluate these analytical solutions. The comparison of these three methods is satisfying. When $t_\mathrm{p} = 0.40\,\mathrm{s}$, the arch after rocking for a while returns to its initial position ($\varphi = 0$). On the other hand, when $t_\mathrm{p} = 0.44\,\mathrm{s}$, the rotation φ gradually increases leading to overturning.

Similar results of the comparison between two methods of analysis can be extracted when the excitation period is significantly lower. In this way, a new set of rectangular pulses is adopted with duration values 0.20 and 0.27 s. Time histories of the computational solution of Eq. (9) (*Mathematica*) and comparison with the finite element analysis (*Abaqus*) are illustrated in Fig. 11.

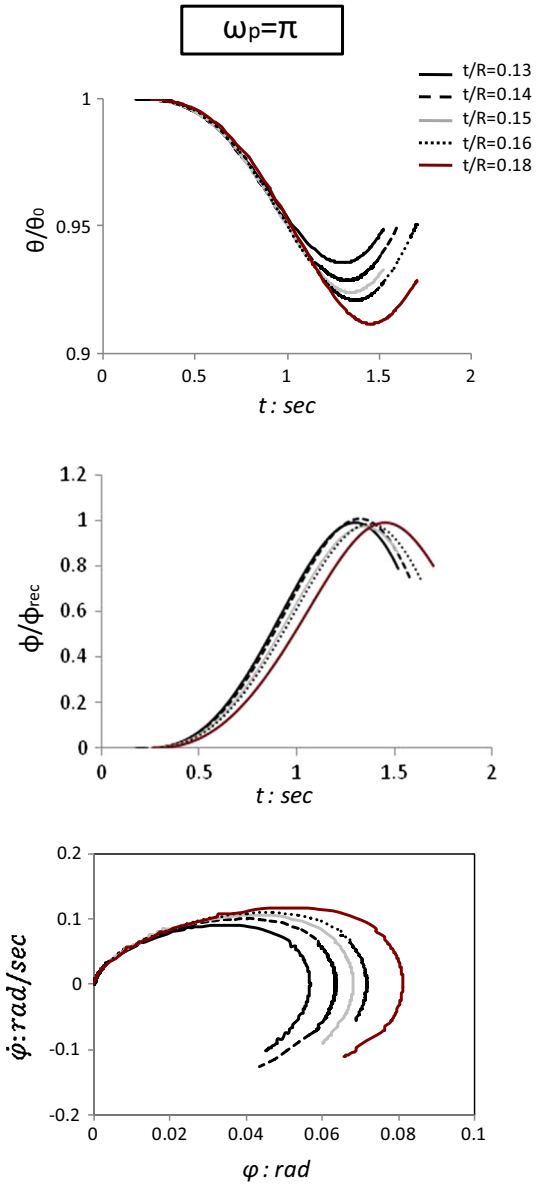

Fig. 8 Time histories of the normalised angle θ_{AB}, rotation ϕ and phase diagram of a marginally safe arch subjected to sine pulses ($\omega_{\mathrm{p}} = \pi$) for different values of t/R

5 Applicability and limitations

5.1 Influence of the number of blocks

As mentioned above, the hinge locations are assumed fixed during the rocking vibration. The accuracy of the simplification of a four-hinge mechanism is strengthened by computational and experimental results of earlier studies [10]. The applicability of the four-hinge model is investigated herein by conducting analyses through finite element formulation of a seven-rigid block arch. The same type of pulses used in previous analyses is implemented to simulate ground excitation at the base of the model: (a) one-sine pulses and (b) rectangular pulses. Time histories of angle θ_{AB} in the case of a seven-block arch are in a good agreement with the numerically and analytically computed results of a three-block arch as illustrated in Fig. 12. On the

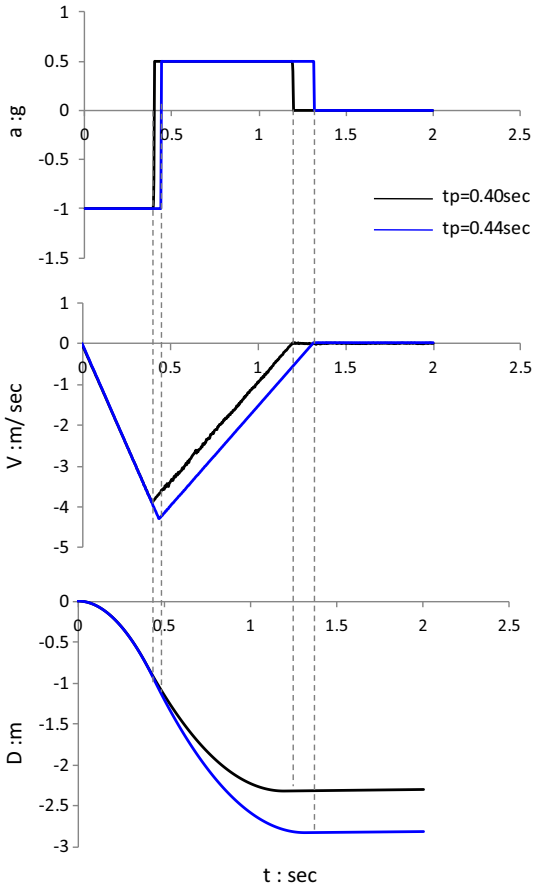

Fig. 9 Impact of the impulses, with durations $t_p = 0.40, 0.44$ s and acceleration magnitude $a = 1g$, on velocity and displacement time histories of the arch base

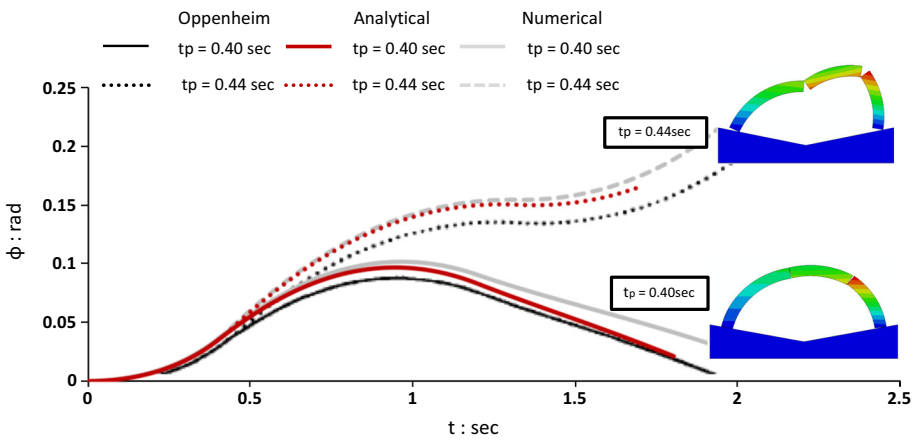

Fig. 10 Response to idealised ground motion pulse

other hand, in the case of rectangular pulses, the results indicate not only a larger rotation ϕ (especially for $t_p = 0.27$ s) but also a slower return from θ to θ_0 (Fig. 13). Although it is a complicate task to describe the behaviour of each voussoir of the arch, it is also challenging for future research.

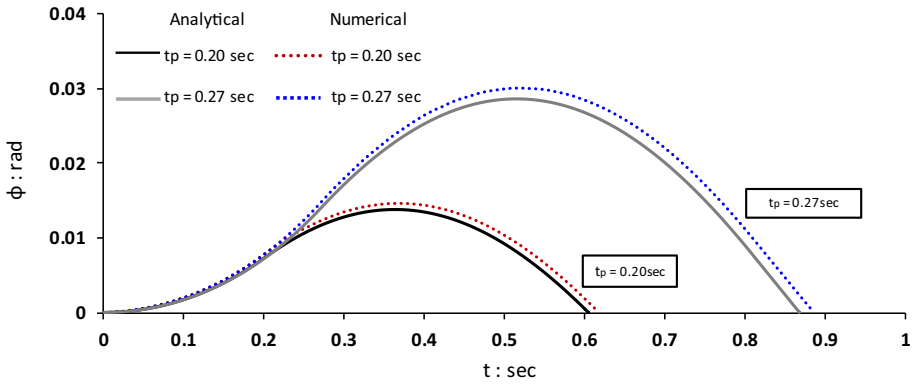

Fig. 11 Response to idealised ground motion pulse

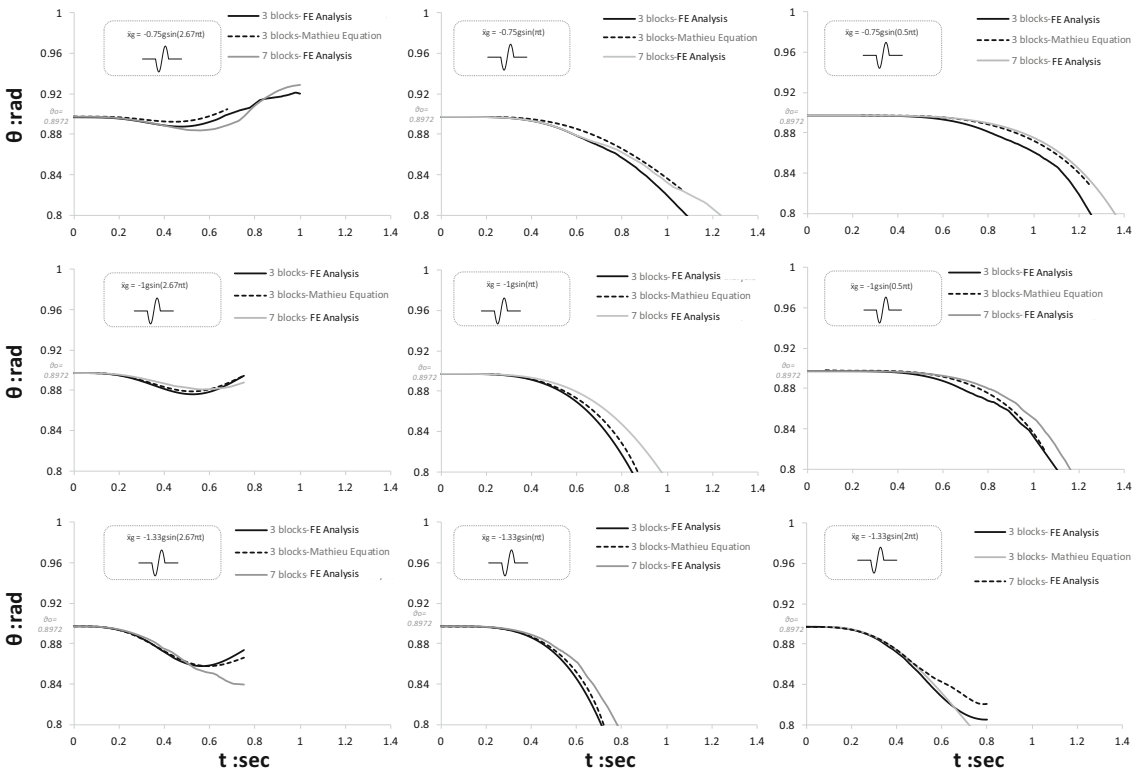

Fig. 12 Time histories of the angle θ_{AB} under one-sine pulse base excitation: (line 1) $a_{\mathrm{p}} = -0.75g$, $T_{\mathrm{p}} = 0.75, 2, 4\,\mathrm{s}$, (line 2) $a_{\mathrm{p}} = -1g$, $T_{\mathrm{p}} = 0.75, 2, 4\,\mathrm{s}$, (line 3) $a_{\mathrm{p}} = -1.33g$, $T_{\mathrm{p}} = 0.75, 1, 2\,\mathrm{s}$: comparison between arches consisting of three blocks and seven blocks

5.2 Influence of sliding

The effect of friction on the arch response is also investigated. Influence of sliding has met only limited investigation in the past. A few experimental studies have revealed that the results are not generally influenced as initiation of sliding is difficult to occur. According to the results of finite element analyses, the coefficient of friction (μ) has practically no appreciable effect on the arch behaviour in the case of a three-block arch imposed on both rectangular and sine pulses (Figs. 14, 15 left). On the other hand, for an arch of seven voussoirs, some differentiations are observed. Particularly, from Fig. 14 (right), where time history of rotation ϕ is depicted, it is extracted that a low coefficient of friction ($\mu = 0.51$) is accompanied with larger rotations. It is important to note that such values of μ are less than the typical ones. The numerical investigation continues with specific sine pulses (Fig. 15 left). In the first half cycle of high-frequency shaking, the coefficient of friction does not play

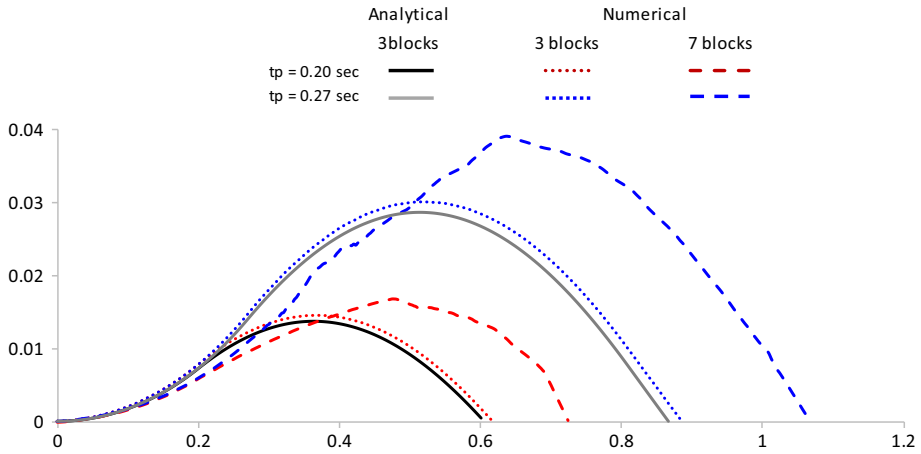

Fig. 13 Response to idealised rectangular pulses for arches consisting of three and seven blocks

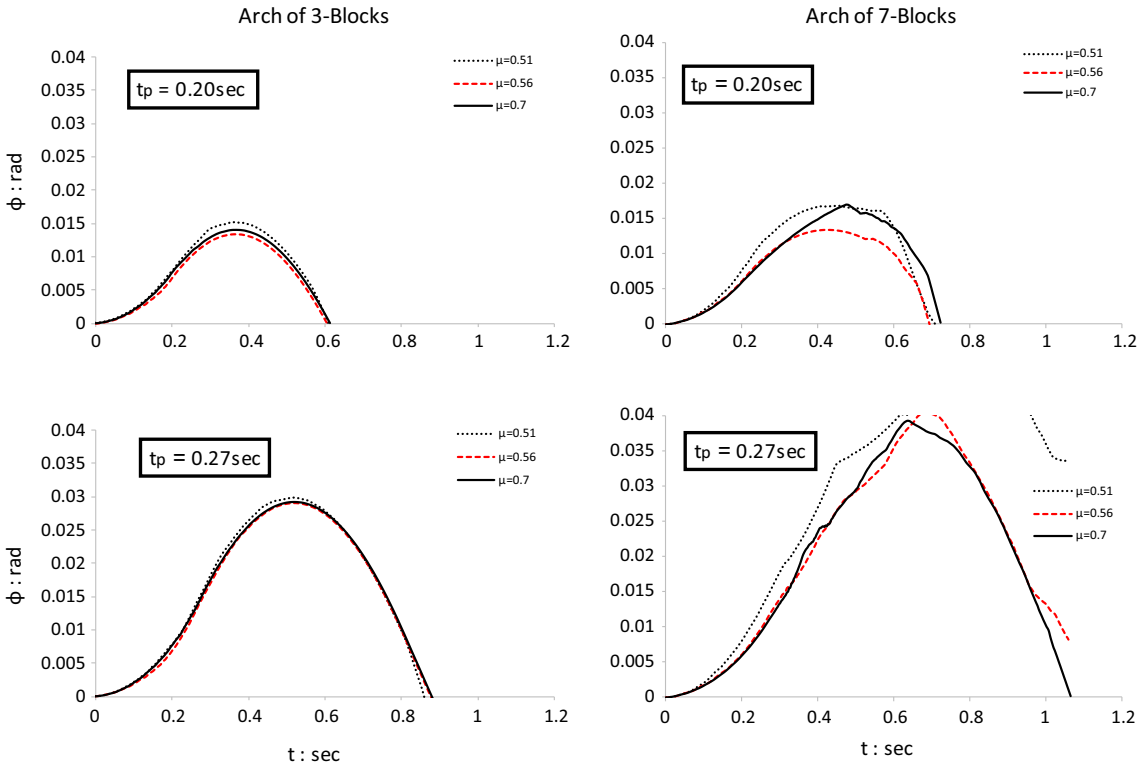

Fig. 14 Effect of the coefficient of friction on the behaviour of arches consisting of three (left column) and seven blocks (right column) under rectangular pulses

any particular role. Larger deviations in angle θ_{AB} under various coefficients are observed for higher values of acceleration amplitudes a_p. Differentiations in rotations or angles are totally expected due to accumulated small displacements on each joint.

From the investigation that took place, as presented on the diagrams below, sliding does not essentially affect the collapse mechanism. Small-scale experiments offer a strong corroboration to the above conclusion. De Jong et al. [10] performed harmonic and seismic testing on two geometrically different arches finding out that no sliding occurs. They remarked that "failure occurred as a result of hinging and rocking".

To this end, the above findings give a glimpse of how the number of blocks and coefficient of friction affect the arch response. They should await considerably more analytical and experimental testing before being evaluated.

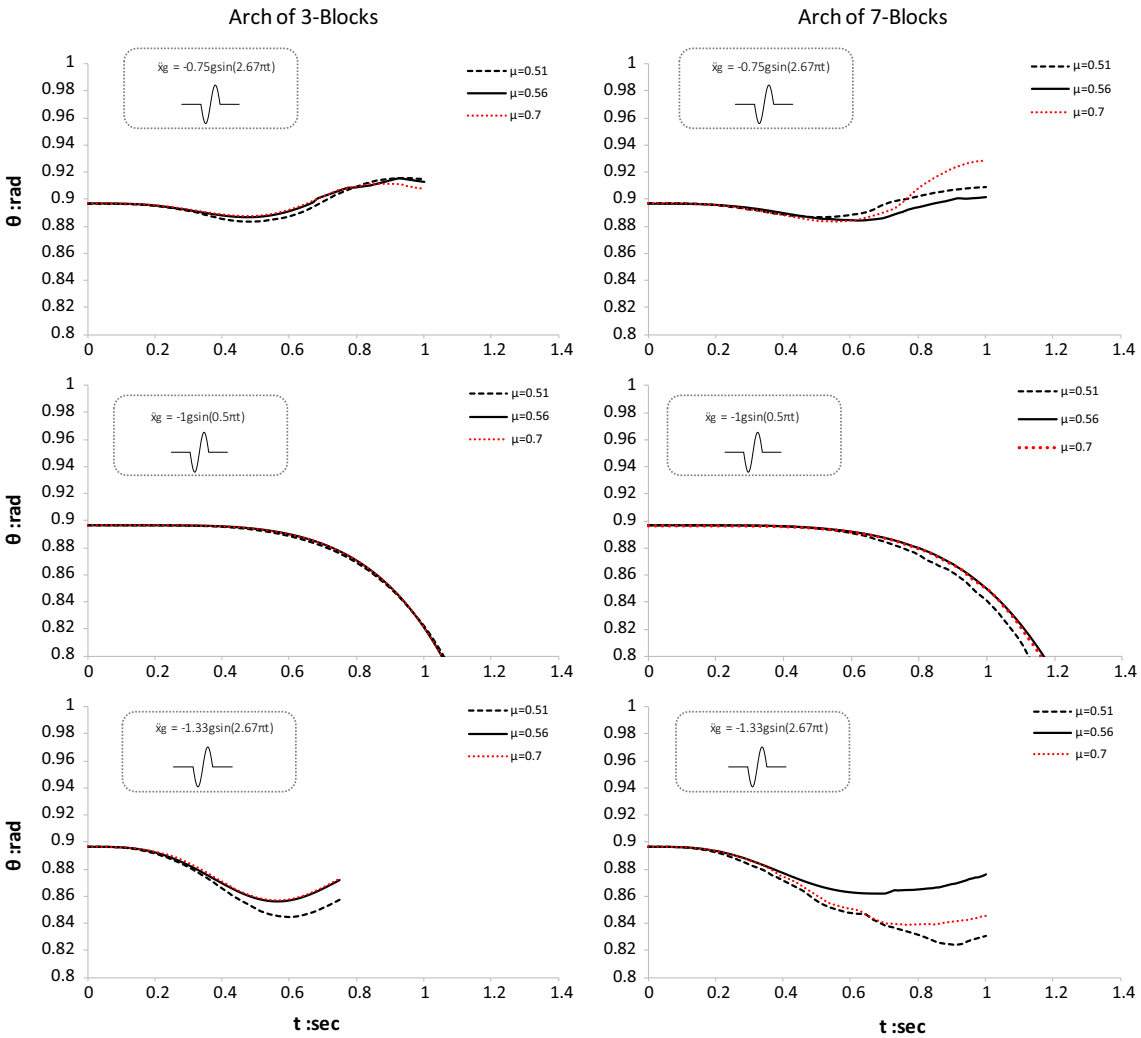

Fig. 15 Effect of the coefficient of friction on the behaviour of arches consisting of three (left column) and seven blocks (right column) under sine pulses

6 Conclusions

The study revisits the dynamic behaviour of a part-circular masonry arch subjected to ground motion, as introduced by Oppenheim in 1992. The examined model, under horizontal acceleration applied at its base, is transformed into predefined rigid body assemblies. This concept of arch modelling founds a direct application to monumental masonry arches. In such stiff structures, rocking rotation even in low-amplitude levels is most often undesirable as it may lead to severe permanent displacements accompanied with possible dislocation of the arch axis, and sometimes to general instability of the structure. It is therefore of great importance to develop simplified procedures for estimating the levels of the low-amplitude response. In this context, simplified analytical techniques are applied to calculate the linear response. These methods comprise both closed-form solutions and numerical integration of the equation of motion. Applicability of linearised response is evaluated mainly through comparison with rigorous two-dimensional finite element analysis. Moreover, where available, the results are compared with those of the literature. Near-source earthquake shaking is represented with idealised cycloidal and rectangular pulses. In addition, constant acceleration pulses are involved.

A general solution of the resulting linear equation of motion, extracted with the Lagrangian method, suitable for any arch geometry is presented. The impact of the gravitational and the external forces to the system, represented by the coefficients, $F(\phi)$ and $P(\phi)$, respectively, is also discussed. Then, a first application of

this general solution is given through the examination of constant acceleration pulses. Simplified forms of the rotation θ_{AB} (Lagrangian variable) with respect to time are presented.

One-sine pulses are also introduced to represent ground excitation. In this respect, a linear second-order homogeneous differential equation of motion is derived, similar to Mathieu equation. According to superposition principle, each solution of the Mathieu equation is a linear combination of two independent solutions, thus allowing for a closed-form solution to be obtained. In parallel, numerical integration of the equation of motion is involved to compute the response. A parametric comparative study is presented for different values of the peak ground acceleration and excitation period. Nonlinear finite element analysis in the time domain is also employed to further strengthen the comparison. The results reveal a close agreement between these methods and justify the applicability of the linear simplification of the response. The benefit of the Mathieu equation to easily derive reliable results in large amounts is applied to the study of the overturning response of the arch. The parametric study reveals that overturning of the arch according to the minimum overturning acceleration spectrum is more sensitive to high values of a_{p} and low values of T_{p}. Another interesting finding is that overturning and imminent collapse occur without impact.

Rectangular asymmetric pulses are also involved in the study of the earthquake response. The type of the pulse and the values chosen are those used by Oppenheim so that a comparative study is possible. The results indicate convergence between linear analytical and nonlinear finite element methods. The reliability of these results is further strengthened by the comparison with Oppenheim's results for rectangular pulses.

References

1. Coulomb, C.A.: Theorie des machines simples (1821)
2. Couplet, P.: De la poussée des voûtes, Histoire de l'Académie Royale des Sciences, pp. 79–117, 117–141. Académie royale des sciences, Paris (1729, 1730)
3. Heyman, J.: The stone skeleton. Int. J. Solids Struct. **2**, 249–279 (1966)
4. Heyman, J.: The Masonry Arch. Ellis Horwood, Chichester (1982)
5. Heyman, J.: The safety of masonry arches. Int. J. Mech. Sci. **11**, 363–385 (1969)
6. Oppenheim, I.J.: The masonry arch as a four-link mechanism under base motion. Earthq. Eng. Struct. Dyn. **21**, 1005–1017 (1992)
7. Housner, G.W.: The behaviour of inverted pendulum structures during earthquakes. Bull. Seismol. Soc. Am. **53**(2), 403–417 (1963)
8. Clemente, P.: Introduction to dynamics of stone arches. Earthq. Eng. Struct. Dyn. **27**, 513–522 (1998)
9. De Lorenzis, L., DeJong, M., Ochsendorf, J.: Failure of masonry arches under impulse base motion. Earthq. Eng. Struct. Dyn. **36**(14), 2119–2136 (2007)
10. De Jong, M., De Lorenzis, L., Adams, S., Ochsendorf, J.: Rocking stability of masonry arches in seismic regions. Earthq. Spectra **24**, 847–865 (2008)
11. Alexakis, H., Makris, N.: Limit equilibrium analysis and the minimum thickness of circular masonry arches to withstand lateral inertial loading. Arch. Appl. Mech. **84**, 757–772 (2014)
12. Apostolou, M.: Soil–structure interaction under strong seismic moment: material and geometric nonlinearity. Dissertation, National Technical University of Athens (2011)
13. Zhang, J., Makris, N.: Rocking response of free-standing blocks under cycloidal pulses. J. Eng. Mech. ASCE **127**(5), 473–483 (2001)
14. Makris, N., Roussos, Y.: Rocking response and overturning of equipment under horizontal pulse-type motions. Rep. No. PEER- 98/05, Pacific Earthquake Engrg. Res. Ctr., University of California, Berkeley, CA (1998)
15. Coisson, R., Vernizzi, G., Yang, X.: Mathieu functions and Numerical solutions of the Mathieu equation. In: IEEE Proceedings of the International Workshop on Open Source Software for Scientific Computation, pp. 3–10 (2009)
16. Langer, R.: The solutions of the Mathieu equation with a complex variable and at least one parameter large. Trans. Am. Math. Soc. **36**(3), 637–695 (1934)